RESTORATION OF ASTRONOMICAL IMAGES BY WAVELET TECHNIQUES

Vinicius S. Monego

vinicius.monego@inpe.br

Instituto Nacional de Pesquisas Espaciais (INPE)

Av. dos Astronautas 1758, Zip: 12227-010, São José dos Campos, SP, Brazil

Alice J. Kozakevicius

alice.kozakevicius@gmail.com

Universidade Federal de Santa Maria (UFSM)

Av. Roraima 1000, Zip: 12227-000, Santa Maria, RS, Brazil

Haroldo F. Campos Velho

haroldo.camposvelho@inpe.br

Instituto Nacional de Pesquisas Espaciais

Av. dos Astronautas 1758, Zip: 12227-010, São José dos Campos, SP, Brazil

Abstract. *Image restoration, an important application of inverse problem techniques, is relevant for remote sensing, surveillance and security, medicine, material science, research on biology, entertainment industry, and more recently for aerial drone autonomous navigation. Our focus is on astronomical images. Indeed, observational astronomy is fully dependent on image interpretation. Therefore, image restoration techniques applied to astronomy is a relevant research topic in this field. Here, Several wavelet schemes are applied for astronomical images restoration, ranging from the orthogonal wavelets, including Haar, Daubechies, and Symlet families, to biorthogonal wavelets. Different thresholding schemes are assumed to analyze the resulting wavelet decomposition, assuming as input data RGB images with high noise levels. The results are evaluated by using structural image similarity as the comparative metric for different schemes to image restoration.*

Keywords: Astronomical images, image restoration, wavelet transform, wavelet shrinkage, filtering.

1 Introduction

The process of image reconstruction, restoration, or mitigation of degradation effects has motivated a great amount of research with many applications in science and technology: material science, medical tomography, biology, remote sensing, geophysics, autonomous navigation, and robotics are some examples. This type of signal analysis can also be treated as an inverse problem, belonging to the class of ill-posed ones.

A set of factors implies in the image degradation process, such as the distortion by the optical system, motion blur, light absorption during photon traveling, to mention a few. There is a large literature on this subject–see Gonzalez and Woods (1992) [1] and Beterro and Boccacci's (1998) [2] books, in which several methods for image restoration are described. In a previous contribution [3], we investigated four different techniques: truncated singular value decomposition, Tikhonov regularization, neural network restoration, and wavelet filtering. Previously the main goal in [3] was to present the application of four modern approaches for image restoration. Here, the focus is to do a better exploration on the wavelet based schemes.

By astronomical images, we refer to visual signals captured by space telescopes. These signals may represent galaxies, planets and other celestial bodies. This type of image is characterized by high resolution and a considerable amount of dark pixels. They may or may not contain a high variance of pixels. Images of galaxies, for example, may have more variance of brightness, while images of planets are usually more dull. Thus, computational performance is one key factor in order to efficiently analyze them.

In the last 20 years, wavelet transforms have been considered as an efficient methodology in signal and image analysis, specially for filtering and denoising tasks [4]. In this sense, reconstruction schemes based on wavelet transforms can be considered as an competitive alternative for treating astronomical images. In the current work, we investigate the impact of the chosen wavelet family in the analysis, considering orthonormal basis (Haar, Daubechies and Symlets) and biorthogonal (Biorn,n) as well. Besides the transform basis, the choice of the thresholding strategy, which is the main part of the analysis, is also explored. The classical Soft thresholding

and Hard thresholding schemes [5] are combined with techniques for estimating the threshold value (VisuShrink, BayesShrink). And the cycle spin approach, proposed by Coifman and Donoho [6], is incorporated to diminish distortions caused on the boundaries of the image due to the Gibbs phenomena.

In order to organize the presentation of our contribution, the topics are distributed as follows. In Section 2, relevant topics from the considered wavelet families are briefly summarized. The soft and hard threshold functions are also formulated in Subsection 2.1, as well as the estimation of the threshold value and the contribution of the cycle spin procedure. In Section 3, some characteristics about the astronomical images are mentioned and the proposed denoising methodology is also presented. Finally in Section 4, the designed numerical simulations are discussed and the results are presented.

2   Wavelet Filtering

The fast discrete wavelet transform, proposed by Mallat [7], is an implementation based on discrete convolutions involving the input signal $x[N]$ (with $N = 2^{jmax}$ elements) and filters $h[k]$ and $g[k]$. These filters are uniquely associated to the wavelet family, preserving the relationship of scaling and wavelet functions and their translations in each scale or resolution level. Their size k is associated with the smoothness of the wavelet family.

The scaling coefficients, denoted by C, are obtained from the convolution of $x[N]$ with $h[k]$. The wavelet coefficients, denoted by D in the one dimensional case, result from the convolution of the signal with $g[k]$. The decimated form of the 1D wavelet transform (DWT) is given by the Cascade algorithm [7]. The input signal $x[N]$ is decomposed into J resolution levels ($J \leq jmax$). The 1D wavelet decomposition $\mathbf{v}$ of $x[N]$ is given by $\mathbf{v} = DWT_J(x) = [C_0, D_0, D_1, ..., D_{J-1}]$, in which the vector C_0 contains the scaling coefficients in the lowest level of the transformation ($j = 0$). The vectors $D_0, D_1, ..., D_{J-1}$ contain the wavelet coefficients in each one of the factorization levels, from the first $J - 1$, to the the last and lowest one, indexed by 0.

In the case of the bi-dimensional wavelet transform [7], one standard formulation is the application of the one-dimensional transform by lines and then applied by all columns of the analyzed image (2D data). The main difference now is that after one decomposition level, three blocks of different wavelet coefficients (HL, LH, HH) and only one block with scaling coefficients (C) are generated in the 2D transform. All these blocks have one quarter of the size of the original matrix x. $\mathbf{w} = TWD_1(x) = [C, HL, LH, HH]$. In order to continue the decomposition process, only the scaling coefficient block is further decomposed. The resulting decomposition is a matrix of coefficients defined by blocks $\mathbf{w} = TWD_J(x) = [C_0, HL_0, LH_0, HH_0, ..., HL_{J-1}, LH_{J-1}, HH_{J-1}]$.

Daubechies wavelet

In the case of the orthonormal family of Daubechies wavelet (Db) [8], the filters $h[k]$ and $g[k]$ are also FIR filters and respect the orthogonality of the wavelet basis. In fact, all the properties from the wavelet basis are kept by them, such as compact support and smoothness. The orthonormal family of Daubechies is also characterized by having the maximal number of n vanishing moments for some given support, which also defines the size of $h[k]$ and $g[k]$ as being $k = 2n$. This property is related to the capability of the basis to represent exactly polynomials of degree up to $(n - 1)$ as a linear combination of only the scaling functions at any scale of the transformation. The Daubechies wavelet function is generated by the scaling function, preserving orthogonality among scales.

The *Haar wavelet* is a particular case in the Daubechies wavelet (Db1) family. This mathematical technique to represent a function expanded by an orthonormal basis was also introduced by Alfréd Haar at 1909. The Haar's expansion is cited as the first wavelet basis.

Symlet

Daubechies proposed a modification of the orthonormal wavelet family to increase symmetry, by obtaining functions named *Symlet*. While the name of this family recalls symmetry, this family is only near symmetric. It still maintains the same properties of the Daubechies family, such as compact support and filters with finite size, associated to the vanishing moment property.

Symlets have been employed successfully in signal analysis [9] and are well suited to denoising problems because of their near symmetry [10]. The symmetry property is desirable in denoising applications to preserve phase data [Kovesi].

Biorthogonal wavelet

Another wavelet family, also devised by Daubechies, is the Biorthogonal family. In this wavelet system the decomposition function and the reconstruction function can be different. This implies in the existence of a dual scaling function and a dual wavelet that are combined with the original ones. In this sense, besides the filters

$h[k]$ and $g[k]$, now there also exist $h'[k]$ and $g'[k]$ associated to the dual pair. And the filters considered for the decomposition are therefore distinct from those assumed for the reconstruction.

The Biorthogonal family contains strictly symmetric wavelets at the expense of orthogonality. In other words, it is not possible to have symmetry and orthogonality simultaneously. Therefore, since by construction the basis of the Daubechies and Symlet families are orthogonal, these families cannot be strictly symmetric. In this work, Biorthogonal wavelets are considered in a similar denoising scheme as proposed in [12].

2.1 Wavelet Shrinkage

The two-dimensional wavelet decomposition in J levels of the image x ,

$$\mathbf{w} = TWD_J(x) = [C_0, HL_0, LH_0, HH_0, ..., HL_{J-1}, LH_{J-1}, HH_{J-1}],$$

contains one block of scaling coefficients that represent the main coarse data information. All variations, high frequency associated events, details related to borders and contour and so forth are captured by three blocks of the wavelet coefficients, HL_j, LH_j, HH_j, generated at each level $j = 0, ..., J - 1$.

With the help of the seminal work of Donoho and Johnstone [5], the behavior of the wavelet coefficients when affected by noise was systematically investigated. Since then, analyzing tools have been proposed in order to separate relevant information from those associated to spurious perturbations which are also captured by the wavelet coefficients. The two most well established threshold functions were also proposed in [5]: the *soft thresolding* and *hard thresholding*.

Hard thresholding (Equation 1) is the most intuitive threshold function in the sense of providing an heuristic to discard unnecessary information. Every wavelet coefficient $D_{i,j}$ (assuming values from any of the blocks HL_j, LH_j, HH_j) that is below the threshold value λ will be truncated, while any other value will be preserved.

$$thr_\lambda^S(D_{j,k}) = \begin{cases} 0\,, & \text{if } |D_{j,k}| \leq \lambda \\ |D_{i,j}|\,, & \text{if } |D_{i,j}| > \lambda. \end{cases} \tag{1}$$

Soft thresholding (Equation 2) is similar to hard thresholding, but it assumes the subtraction of λ from the wavelet coefficients above λ. This "shrinks" the signal representation, implying in a more blurred reconstructed image.

$$thr_\lambda^S(D_{j,k}) = \begin{cases} 0\,, & \text{if } |D_{j,k}| \leq \lambda \\ sign(D_{j,k})(|D_{j,k} - \lambda|)\,, & \text{if } |D_{i,j}| > \lambda. \end{cases} \tag{2}$$

The choice of the threshold value, λ, determines the quality of the denoising or compression procedure. Two λ estimators considered in this work are the VisuShrink [5] and BayesShrink [13] schemes.

The VisuShrink approach uses a universal threshold, which is measured by Equation 3. It is proportional to the size of the image $n = (M \times N)$ and the standard deviation σ of the noise, estimated by the wavelet decomposition.

$$\lambda_{vs} = \sigma\sqrt{2 * \log n}. \tag{3}$$

The universal threshold is generally a poor choice because it is often too large and removes too much of relevant signal information related to the contours of the image. This results in oversmoothing the image. One way to control this issue is to tweak the standard deviation, such as using a fraction of it. Another way is to use adaptive threshold estimators, which uses local information from each sub-band $Y = (HL_j, LH_j, HH_j)$ to estimate a locally adapted λ for each sub-band (λ_Y). One example of an adaptive threshold estimator method is the BayesShrink estimator (Equation 4), which will be used in this work. Here $n = (M_j \times N_j)$ is the size of the sub-band Y on level j.

$$\lambda_Y = \frac{\sigma^2}{\sigma_X}, \quad \sigma_X = \sqrt{max(\sigma_Y^2 - \sigma^2, 0)}, \quad \sigma_Y^2 = \frac{1}{n^2}\sum_{i,j=1}^n Y_{ij}^2. \tag{4}$$

The estimation of the standard deviation σ is another issue, since it is an unknown information in a real scenario. It can be computed assuming the wavelet coefficients from all wavelet blocks, as proposed initially in [5]. Equation 5 was also proposed in [5] as a way to estimate σ for one-dimensional data, assuming D_0 the wavelet coefficients from the coarsest block of the decomposition. This technique can also be used for 2D data, by replacing D_0 with the wavelet coefficients for each sub-band $Y = (HL_j, LH_j, HH_j)$ at different levels, as well.

$$\sigma \approx \frac{Median(|D_0|)}{0.675}. \tag{5}$$

Therefore, the wavelet denoising approach can be summarize with the following steps:
1. Decomposition the image x in j levels: $\mathbf{w} = TWD_J(x)$,
2. Choose the threshold function and the threshold value,
3. Thresholding the wavelet coefficient blocks, obtaining $\hat{HL}_0, \hat{LH}_0, \hat{HH}_0, ..., \hat{HL}_{J-1}, \hat{LH}_{J-1}, \hat{HH}_{J-1}$,
4. Apply the Inverse wavelet transform (IWT) to the thresholded wavelet blocks together with the scaling coefficients C_0. The resulted $\tilde{x} = IWT[C_0, \hat{HL}_0, \hat{LH}_0, ..., \hat{LH}_{J-1}, \hat{HH}_{J-1}]$ is the restored image.

Cycle spin

The decimated formulation of the discrete wavelet transform which is implemented through the Cascade algorithm is not translation invariant. This formulation may introduce artifacts in the image's border specially because of the assumption of periodic boundary extension while doing the filter convolution with values on the image boundaries. This is known as the Gibbs Phenomenom. One way to solve this problem is considering the *cycle spin* [6] procedure, given as:
1. Shift rows and columns by s places (pixel positions).
2. Denoise the shifted image
3. Unshift the image, take the average between this denoised signal and the original denoised signal.

3 Wavelet Denoising

The considered digital image is represented as a matrix L, whose discrete coordinates (x, y) are the row and column entries of L. These coordinates are the *pixels'* addresses. The matrix values $L(x, y)$ are the gray levels (from white to black) per pixel (per position) [1]. A color image is a composition of three images, one in red, one in green and the other in blue (RGB) color, each one having its corresponding intensity levels for each pixel.

Data Preprocessing

The color images are converted to YCbCr color channel, as similarly done in [12]. The main advantage of using color channels based on luminance is the gain in performance, since only the luminance channel (Y) has to be denoised. We also note that different color channels may give better results, as pointed out in [14].

Noisy data

When noise is present in the image, we are dealing with a degraded image. The most common kind of degradation associated with image acquisition tools is Gaussian noise, which is the type of noise we will consider in this work. To validate the proposed denoising schemes, we will artificially degrade clean astronomical images with Gaussian noise. The chosen noise type was an additive Gaussian noise with 10% of variance. The performance of the denoising procedure is presented in Section 4, assuming various wavelet families and different threshold functions

Metrics

In agreement with the specialized community, the chosen metrics to analyze the performance of the denoising procedure are the Normalized Root Mean Square (NRMSE), the Peak Signal to Noise Ratio (PSNR) , and the Structural Similarity Index Measure (SSIM). Assuming I the reference image and $\tilde{I}$ being the reconstructed one and E as being the expectation, computed in the discrete form, the metrics are given by:

$$MSE = E\{(I - \tilde{I})^2\}, \quad NRMSE = \frac{\sqrt{MSE}}{MAX(I)}, \quad PSNR = 10 \log \frac{MAX(I)^2}{MSE}. \tag{6}$$

DWT

For the wavelet transform, which is the first step of the denoising procedure, we assumed three different wavelet families: Daubechies, Symlet and Biorthogonal. More precisely, we chose Haar (db1) and Daubechies with 10 vanishing moments (db10) as representatives from the Daubechies wavelets. The Biorthogonal 6.8 and Symlet 4, which has basis functions which closely match Biorthogonal's 3.3. The Haar wavelet is the most popular

choice for denoising, due to its simplicity and efficiency. And Biorthogonal 6.8 is similar to db10 in shape and filter's size. Given the multiresolution property of the wavelet transform, a parameter that has to be determined is the number of decomposition levels of the transformation. We chose it according to Equation 7 [14]:

$$0 \leq j \leq \frac{\log_2 M + \log_2 N}{4} - 1, \tag{7}$$

being M and N the height and width of the image, respectively. Therefore, the assumed value is $j = 3$. The algorithms considered in the simulations are provided by the *scikit-image* [15] project, version 0.16.2.

Cycle spin

We applied a value of 5 different shifts, starting from $s = 1$ to $s = 5$. Because the Gibbs Phenomenom is strong closer to the image's border, it is enough to apply only a small number of shifts to bring the pixels at the border closer to the center. Larger number of shifts will add computational overhead while the benefits will not be as noticeable as we wanted. This is because the Gibbs Phenomenom is weaker the farther we are from the border. For this reason, we choose the range from 1 to 5 displacements (s).

4   Results and Discussions

Our test images were chosen from HubbleSite, cropped and rescaled to size 512×512. The experiments were performed by several astronomical images: galaxy, planets (Saturn and Jupiter), and solar loop. For the sake of space, only the galaxy restoration is shown in this paper. The image is from the NGC 3147 galaxy, and it can be seen in Figure 1(a). It contains a significant amount of variance around the disk, with speckles representing stars. Its degraded counterpart, with a Gaussian noise of zero mean and $\sigma^2 = 0.1$, can be seen in Figure 1(b).

We found the best overall results by the combination of BayesShrink and soft thresholding for the NGC 3147 image, and VisuShrink and hard thresholding for the Jupiter image. Figure 2 displays the resulting denoised images for all the four aforementioned wavelets. Note that the Haar wavelet is able to recover the dark surroundings more faithfully to the original image. This is because the Haar wavelet is naturally designed to capture sharp variations, since the wavelet function itself presents a jump. All the transforms were able to recover much of the star speckles.

Table 1. Wavelet filtering results. A=NRMSE, B=PSNR, C=SSIM. 1=NGC 3147, 2=Jupiter.

W	db10			sym4			Haar			bior6.8		
M	A	B	C	A	B	C	A	B	C	A	B	C
1	0.258	22.544	0.744	0.255	22.618	0.75	**0.252**	**22.726**	**0.757**	0.256	22.612	0.75
2	0.299	19.686	0.4	**0.298**	19.707	**0.402**	**0.298**	19.72	0.4	**0.298**	19.694	**0.402**

In Table 1 we summarized the obtained results for the wavelet denoising procedures, assuming cycle spin with $s = 5$. The performance is presented in terms of the three metrics previously defined: A=NRMSE, B=PSNR, and C=SSIM. The Haar wavelet had the best overall performance, while db10 had the worst. One possible reason for the low performance of db10 might be the size its filters (size $k = 20$) and its lack of symmetry. The structural similarity obtained in the Jupiter image was just over half than that obtained in the NGC 3147 image.

We also check the contribution for the cycle spin technique and color channel conversion in Table 2 for the Haar wavelet. As seen, cycle spin with 5 shifts may increase 0.6dB in PSNR for the NGC 3147 image, and 0.3dB for the Jupiter image, and around 0.5% similarity for both.

5   Conclusions

Wavelet techniques were applied for astronomical image reconstruction. The denoising procedures performance were analyzed employing different wavelet basis considering the discrete wavelet transform. Orthonormal wavelets were aaplied from the Daubechies family (Haar and db10), as well as Symlets and biorthogonal wavelets. Two thresholding methods (soft threshold and hard threshold) have been combined with two threshold estimators: one static (VisuShrink) and the other adaptive (BayesShrink) in order to discard spurious information from the images. The cycle spin strategy was also included in the denoising procedure to diminish the distortions caused by the
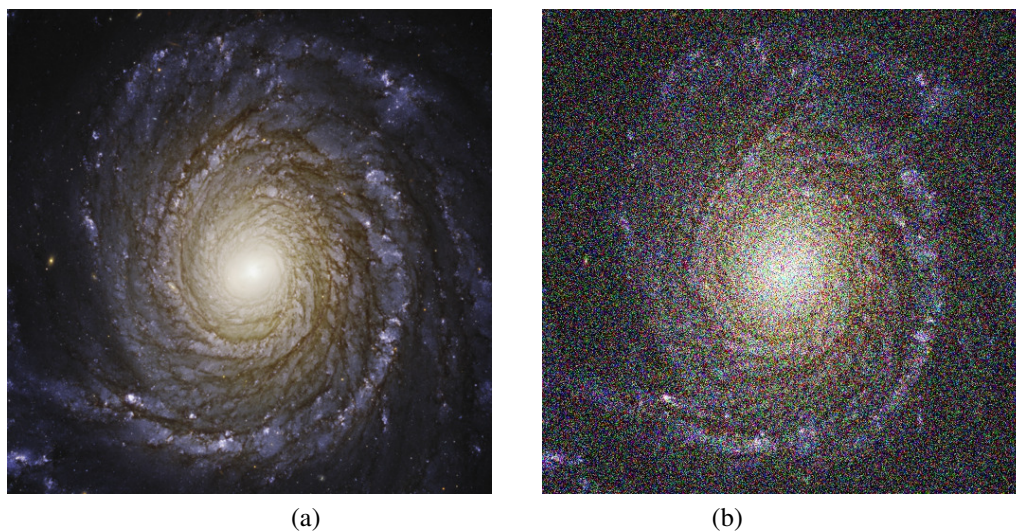
(a)   (b)

Figure 1. NGC 3147 image: (a) original, (b) noisy.

(a)   (b)

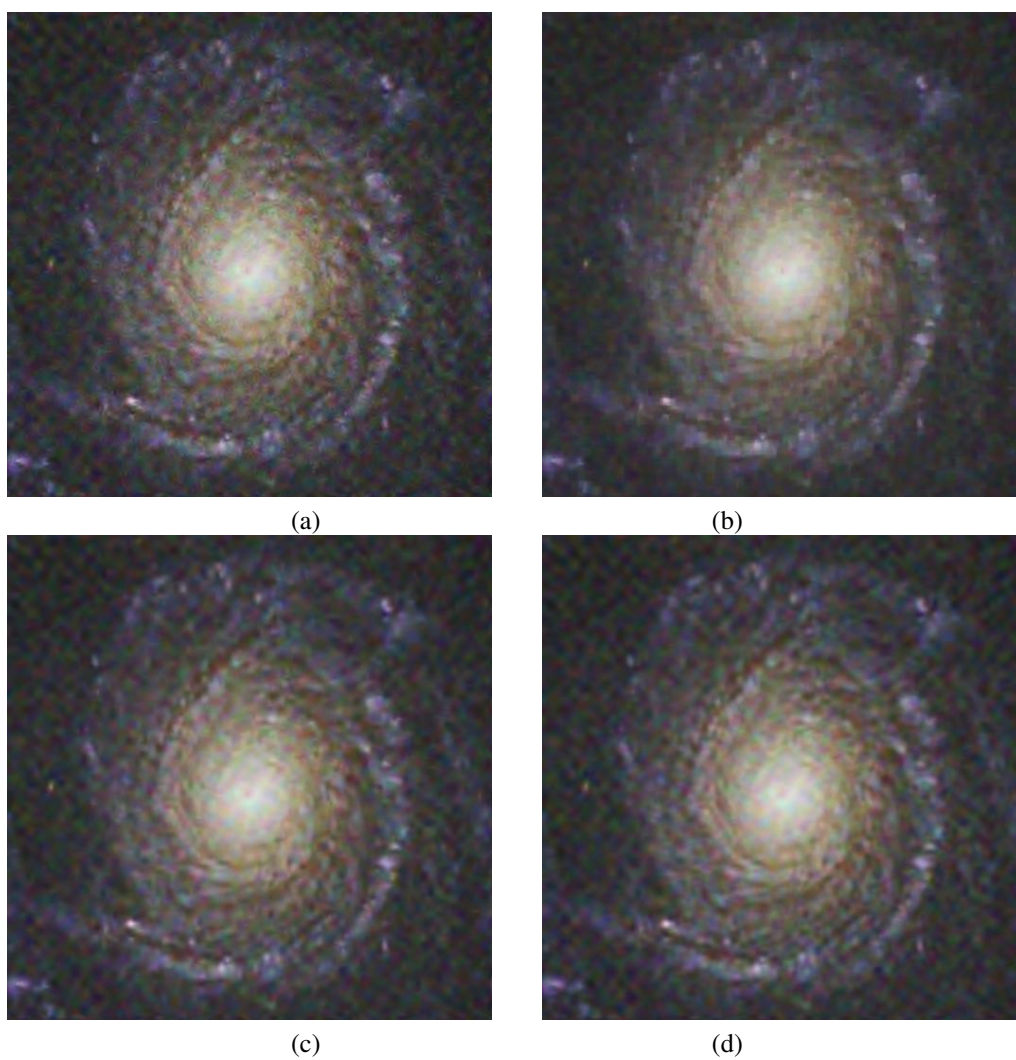(c)   (d)

Figure 2. NGC 3147 restoration by Wavelet filtering: (a) Bior6.8, (b) Haar, (c) Sym4, (d) Db10.

Table 2. Wavelet filtering results.

Procedure	s=0 + YCbCr			s=5 + RGB			s=5 + YCbCr		
Metric	NRMSE	PSNR	SSIM	NRMSE	PSNR	SSIM	NRMSE	PSNR	SSIM
NGC 3147	0.271	22.111	0.69	0.256	22.581	0.742	0.252	22.726	0.757
Jupiter	0.308	19.433	0.354	0.298	19.712	0.399	0.298	19.72	0.4

Gibbs phenomena. The cycle spin has an effective contribution was highlighted by the presented performances. Despite being the only discontinuous one from the orthonormal wavelets, the Haar wavelet is still a reasonable and competitive choice for astronomical images. The Haar wavelet was able to efficiently treat the dark pixels, which are prevalent in this type of image. Another observation is that the choice of wavelet family has not been as impactful as the choice of threshold methods and associated values. The other technique explored was the color channel conversion, which had a relevant contribution for increasing the quality of the denoising procedure.

Authorship statement. This section is mandatory and should be positioned immediately before the References section. The text should be exactly as follows: The authors hereby confirm that they are the sole liable persons responsible for the authorship of this work, and that all material that has been herein included as part of the present paper is either the property (and authorship) of the authors, or has the permission of the owners to be included here.

References

[1] Gonzalez, R., Gonzalez, R., Gonzalez, R., Woods, R., & Woods, R., 1992. *Digital Image Processing*. Addison-Wesley world student series. Addison-Wesley.

[2] Bertero, M. & Boccacci, P., 1998. *Introduction to Inverse Problems in Imaging*. Institute of Physics, London.

[3] Shiguemori, A. P., Dantas, M. S., Shiguemori, E. H., Kozakevicius, A. J., Monego, V. S., Ruiz, R. S. R., Strieder, C., & Campos Velho, H. F., 2017. Methods for astronominal image restoration. In *Iberian Latin-American Congress on Computational Methods in Engineering*.

[4] Fan, L., Zhang, F., Fan, H., & Zhang, C., 2019. Brief review of image denoising techniques. *Visual Computing for Industry, Biomedicine, and Art*, vol. 02, pp. 1–12.

[5] Donoho, D. L. & Johnstone, J. M., 1994. Ideal spatial adaptation by wavelet shrinkage. *biometrika*, vol. 81, n. 3, pp. 425–455.

[6] Coifman, R. R. & Donoho, D. L., 1995. Translation-invariant de-noising. pp. 125–150. Springer-Verlag.

[7] Mallat, S., 2008. *A Wavelet Tour of Signal Processing*. Academic Press, 3 edition.

[8] Daubechies, I., 1992. *Ten lectures on wavelets*, volume 61. Siam.

[9] S.S.Gornale, R.R.Manza, Humbe, V., & K.V.Kale, 2007. Performance analysis of biorthogonal wavelet filters for lossy fingerprint image compression. *INTERNATIONAL JOURNAL OF IMAGING SCIENCE AND ENGINEERING (IJISE)*, vol. 01, pp. 16–20.

[10] Kumari, S., 2012. Effect of symlet filter order on denoising of still images. *Advanced Computing An International Journal*, vol. 3, pp. 137–143.

[Kovesi] Kovesi, P. Phase preserving denoising of images.

[12] S, M., Abraham, L., & Moni, R., 2015. Multiresolution color denoising using biorthogonal wavelets for satellite images. *International Journal of Engineering and Advanced Technology*, vol. 05, pp. 28–34.

[13] Chang, S. G., Yu, B., & Vetterli, M., 2000. Adaptive wavelet thresholding for image denoising and compression. *IEEE transactions on image processing*, vol. 9, n. 9, pp. 1532–1546.

[14] Malini, Abraham, L., & Moni, R. S., 2015. Multiresolution color denoising using biorthogonal wavelets for satellite images.

[15] van der Walt, S., Schönberger, J. L., Nunez-Iglesias, J., Boulogne, F., Warner, J. D., Yager, N., Gouillart, E., & Yu, T., 2014. scikit-image: image processing in python. *PeerJ*, vol. 2, pp. e453.